

Dinuclear, Tetranuclear and Chain (Mn^{II}, Co^{II}) Complexes of Multifunctional Hydrazone Ligands – Structural and Magnetic Studies

Peter J. Bettle,^[a] Louise N. Dawe,^[a] Muhammad U. Anwar,^[a] and Laurence K. Thompson*^[a]

Keywords: Hydrazone ligands / Magnetic properties / Cobalt / Manganese

The coordination chemistry of a group of hydrazone-based ligands, modified with carboxylate and heterocyclic terminal donor groups, with Mn^{II} and Co^{II} has been investigated. The multifunctional nature of the ligands allows coordinative flexibility based on the hydrazone core, which is well established to lead to spin-coupled polymetallic assemblies through μ -O_{hydrazone} bridging. Examples of dinuclear, tetra-

nuclear and chain complexes are reported with hydrazone, carboxylate and triazole bridging. Spin exchange through the μ -O and μ -N,N bridging connections leads to antiferromagnetic exchange in most cases, except for the central subunit in the Mn^{II}₄ chain complex, where small (< 90°) bridge angles result in contributing ferromagnetic interactions.

Introduction

Functionalized hydrazone-based ligands have enjoyed considerable success as platforms for the synthesis of square [$n \times n$] ($n = 2-5$) grid complexes by self-assembly, as a result of the contiguous arrangement of coordination pockets containing hydrazone oxygen and nitrogen donor atoms, in addition to donors from terminal groups. A selection of ditopic, tritopic, tetratopic and pentatopic ligands is illustrated in Scheme 1, which produce M₄, M₉, M₁₆, and M₂₅ complexes with Mn^{II}, Co^{II}, Ni^{II}, Cu^{II} and Zn^{II}.^[1] Typically, the end pieces are heterocyclic N-donor groups. The hydrazone oxygen atoms bridge adjacent metal ions leading to spin-exchange interactions. Modifying the hydrazone functionality with, for example, oxime groups leads to the possibility of additional further assembly processes involving the formation of triangular groups of metal ions, which is frequently observed with simple oximes.^[2] This has been observed with the modified hydrazone ligands HL3C and H₂L4, which produce Cu₆ and Cu₃₆ assemblies, respectively, in which the hydrazone groups act in a bridging capacity, but the oxime ends bind three Cu^{II} ions in [Cu₃(μ_2 -NO)₃(μ -O)] triangular groups connected to hydrazone-bridged subunits.^[3,4]

In this study we have used the hydrazone group as a building block and extended it on one end with a carboxylate group and at the other end with a potentially bridging heterocyclic donor group, viz. triazole and pyrazine (Scheme 1; ligands shown in their carboxylic acid form). Reaction with Mn^{II} and Co^{II} salts produced crystalline complexes, in which examples of triazole bridging, carboxylate bridging and pyrazine bridging were observed in

addition to hydrazone bridging. Structures of dinuclear, tetranuclear and chain complexes are described in addition to magnetic data and an analysis of the intramolecular exchange interactions.

Results and Discussion

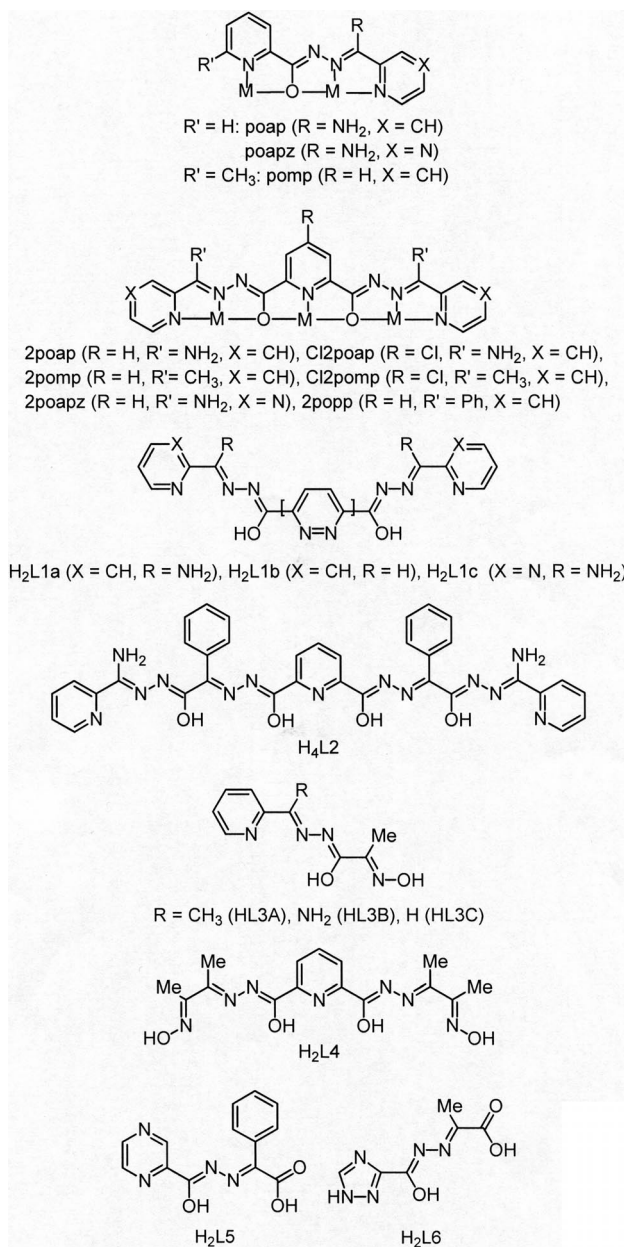
Structural Descriptions

Crystallographic details for 1–4 are listed in Table 5.

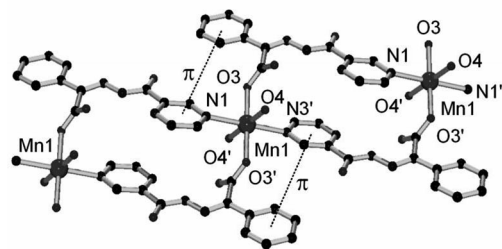
[C₂₈H₃₀MnN₈O₁₀]_n (1)

The structure of **1** is illustrated in Figure 1, and selected bond lengths and angles are listed in Table 1. The structure consists of a 1D chain of metallacyclic rings with each ring comprising two Mn^{II} centres and two ligands. The ligands adopt an unusual open bidentate bonding mode involving a 4-pyrazine nitrogen atom and a carboxylate oxygen atom with two pairs of N and O donor atoms from separate ligands occupying *cis* positions around each six-coordinate Mn^{II}N₂O₄ ion. The other two *trans* coordination sites are occupied by water molecules. The C5–O1 hydrazone bond length is 1.23 Å, which indicates ketone double bond character, with a proton residing on the adjacent nitrogen atom N3. Each ligand therefore behaves as a monoanion, which leads to overall charge neutrality. The Mn–Mn separation is 10.22 Å. One feature, which may in part be responsible for the chain structure, is the proximity of the pyrazine rings within each metallacyclic ring in addition to the pyrazine and phenyl rings. Centroid–centroid distances of 4.40 and 3.78 Å suggest that the pyrazine–phenyl contacts represent the only significant π contacts (Figure 1).

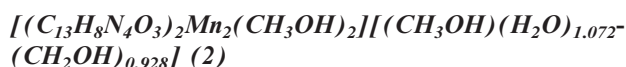
[a] Department of Chemistry, Memorial University, St. John's, NL, A1B3X7, Canada
E-mail: lk.thompson@mun.ca



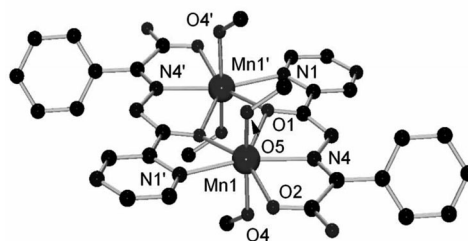
Scheme 1.

Figure 1. Structural representation of **1**.Table 1. Selected bond lengths [Å] and angles [°] for **1**.

Mn1–O3	2.128(3)	O4–Mn1–O4	180.000(1)
Mn1–O4	2.171(3)	O4–Mn1–N1	85.64(12)
Mn1–N1	2.319(4)	O4–Mn1–N1	94.36(12)
O3–Mn1–O3	179.999(1)	O3–Mn1–N1	90.91(14)
O3–Mn1–O4	94.99(12)	O3–Mn1–N1	89.09(14)
O3–Mn1–O4	85.02(12)	O4–Mn1–N1	94.36(12)
O3–Mn1–O4	85.01(12)	N1–Mn1–N1	180.00(1)
O3–Mn1–O4	94.98(12)		

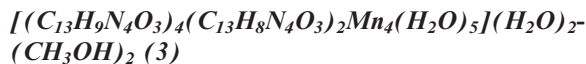


The structure of **2** is shown in Figure 2, and selected bond lengths and angles are listed in Table 2. The structure contrasts sharply with that of **1**, as it is a dinuclear complex with two ligands bridging two seven-coordinate Mn^{II} ions in a [μ-O_{hydrazone}]₂ capacity, with further ligand binding in the pentagonal plane through the carboxylate oxygen, N_{diazine} and pyrazine nitrogen atoms. Axial positions at each Mn^{II} centre are occupied by oxygen atoms from one coordinated methanol molecule and an unusual partial occupancy situation involving a combination of water and methanol at the other position. The excellent data quality for this sample, and the presence of all protons in difference-map positions, revealed this unusual occupancy model expressed in the formula. Figure 2 shows this coordination site represented by just the methanol component (O5). The

Figure 2. Structural representation of **2**.Table 2. Selected bond lengths [Å] and angles [°] for **2**.

Mn1–O4	2.1894(16)	O2–Mn1–O1	138.02(5)
Mn1–O5	2.2176(16)	O1–Mn1–O1	66.05(6)
Mn1–O2	2.2358(17)	O4–Mn1–N4	86.19(6)
Mn1–O1	2.2449(14)	O5–Mn1–N4	92.46(6)
Mn1–O1	2.2606(15)	O2–Mn1–N4	70.65(4)
Mn1–N4	2.2659(17)	O1–Mn1–N4	130.58(5)
Mn1–N1	2.3707(17)	O1–Mn1–N4	67.60(5)
O4–Mn–O5	166.99(5)	O4–Mn1–N1	94.26(6)
O4–Mn1–O2	82.52(5)	O5–Mn1–N1	82.70(5)
O5–Mn1–O2	84.83(5)	O2–Mn1–N1	89.94(5)
O4–Mn1–O1	84.71(5)	O1–Mn1–N1	68.87(5)
O5–Mn1–O1	105.76(5)	O1–Mn1–N1	131.40(4)
O2–Mn1–O1	154.32(4)	N4–Mn1–N1	160.38(5)
O4–Mn1–O1	98.72(5)	Mn1–O1–Mn1	113.95(6)
O5–Mn1–O1	92.69(5)		

Mn–L distances fall in the range 2.18–2.37 Å, typical for Mn^{II}, the Mn–Mn distance is 3.78 Å, and the Mn–O–Mn angle is 114.0°.



The molecular structure of **3** is shown in Figure 3, and selected bond lengths and angles are listed in Table 3. The complex consists of a linear chain of four seven-coordinate Mn centres bound within a group of six ligands. The Mn–L distances fall in the range 2.14–2.38 Å, typical of Mn^{II}. Two tetradentate ligands play the most important role in creating the chain of Mn^{II} ions and binding through their terminal pyrazine N, hydrazone N and O and carboxylate O atoms. The hydrazone oxygen atoms bridge the outer Mn1 atoms to the inner Mn2 atoms, and the terminal carboxylate groups surprisingly link the central pair of Mn centres through μ_2 -O single atom bridging. A third μ -O bridge between Mn2 and Mn2' is provided by a water molecule (O11). The triple oxygen bridging arrangement brings the metal ions into close proximity [Mn2–Mn2' 3.1565(14) Å]. Two other tridentate ligands bind to the outer Mn centres through the hydrazone N and terminal hydrazone O atoms, but once again a μ -O_{carboxylate} atom (O2) bridges Mn1 and Mn2. The Mn–O–Mn angles within the central Mn₂ subunit are < 90° (Mn2–O5–Mn' 89.22°, Mn2–O11–Mn2' 88.00°), whereas angles on the outer Mn₂ subunits are much larger (Mn1–O2–Mn2 103.6°, Mn1–O4–

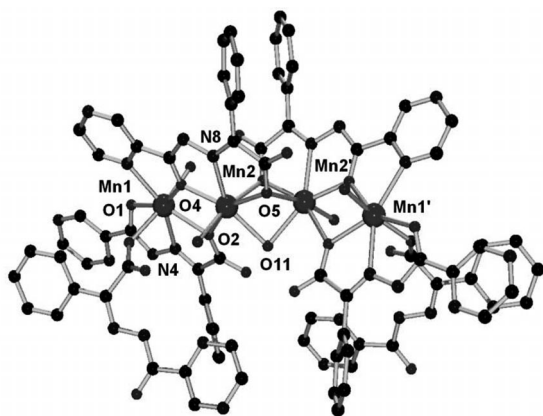


Figure 3. Structural representation of **3**.

Table 3. Selected bond lengths [Å] and angles [°] for **3**.

Mn1–O8	2.141(3)	Mn2–O11	2.272(2)
Mn1–O4	2.145(2)	Mn2–O5	2.298(2)
Mn1–O10	2.156(3)	Mn2–N8	2.306(3)
Mn1–O2	2.282(2)	Mn2–O2	2.341(2)
Mn1–O1	2.295(2)	Mn2–Mn2'	3.1565(14)
Mn1–N4	2.321(3)	Mn1–O2–Mn2	103.57(9)
Mn1–N5	2.372(3)	Mn1–O4–Mn2	115.59(10)
Mn2–O4	2.148(2)	Mn2–O5–Mn2'	89.22(8)
Mn2–O12	2.166(3)	Mn2–O11–Mn2'	88.00(11)
Mn2–O5	2.195(2)		

Mn2 115.6°). This difference is reflected in the magnetic properties (vide infra). The final pair of ligands bind in an unusual monodenate manner to Mn1 and Mn1' through the carboxylate groups and appear to dangle from the ends of the chain. The two bridging ligands bear a –2 charge, whereas the others have –1 charges, thus producing a charge-neutral complex.



The structure of **4** is shown in Figure 4, and selected distances and angles are listed in Table 4. Two distorted octahedral cobalt ions are bound in an almost planar arrangement of two tetradentate ligands, with two deprotonated triazole groups bridging the metal centres. The Co–L distances fall in the range 2.02–2.23 Å, typical of Co^{II}, with short contacts to the triazole nitrogen atoms. The Co–Co distance is 3.75 Å. The Co–N–N–Co torsion angles are < 4°, which indicates essential planarity of the metal ions and the triazole rings. Each triazole ring provides two equatorial nitrogen donors at each Co ion, with water molecules occupying the axial positions and pyruvate oxygen and hydrazone nitrogen donor atoms completing the equatorial coordination. Each ligand has a –2 charge, which results in a charge-neutral species.

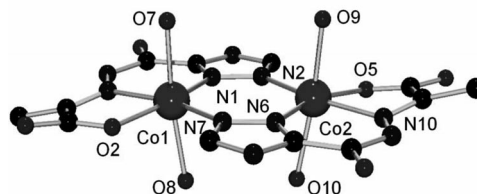


Figure 4. Structural representation of **4**.

Table 4. Selected bond lengths [Å] and angles [°] for **4**.

Co1–O2	2.0447(16)	N7–C o1–N5	165.18(6)
Co1–N1	2.0424(17)	N1–Co1–O8	84.91(6)
Co1–O7	2.0817(15)	O2–Co1–O8	92.60(6)
Co1–N7	2.0880(18)	O7–Co1–O8	173.42(5)
Co1–N5	2.1723(18)	N7–Co1–O8	86.04(6)
Co1–O8	2.1851(14)	N5–Co1–O8	92.20(6)
Co2–O5	2.0261(16)	O5–Co2–N6	161.46(6)
Co2–O5	2.0261(16)	O5–Co2–O9	94.33(6)
Co2–N6	2.0413(17)	N6–Co2–O9	90.58(6)
Co2–O9	2.0943(15)	O5–Co2–N2	87.90(6)
Co2–N2	2.0981(18)	N6–Co2–N2	109.49(6)
Co2–N10	2.1803(18)	O9–Co2–N2	94.99(6)
Co2–O10	2.2299(16)	O5–Co2–N10	78.05(5)
N1–Co1–O2	163.45(5)	N6–Co2–N10	84.56(6)
N1–Co1–O7	91.40(6)	O9–Co2–N10	85.36(6)
O2–Co1–O7	92.47(7)	N2–Co2–N10	165.93(6)
N1–Co1–N7	109.08(6)	O5–Co2–O10	89.95(6)
O2–Co1–N7	87.01(6)	N6–Co2–O10	86.18(6)
O7–Co1–N7	90.03(6)	O9–Co2–O10	174.93(5)
N1–Co1–N5	85.37(6)	N2–Co2–O10	82.45(6)
O2–Co1–N5	78.36(5)	N10–Co2–O10	98.19(6)
O7–Co1–N5	92.94(7)		

Magnetic Properties

Variable-temperature magnetic data for **1** indicate a roughly constant moment of 6.1 μ_B throughout the 2–300 K temperature range, which indicates Curie behaviour consistent with the large distance separating the Mn ions. Variable-temperature magnetic data for **2** are shown in Figure 5 as plots of molar susceptibility and moment as a function of temperature. The overall smooth drop in moment with decreasing temperature indicates the presence of intramolecular antiferromagnetic exchange, and the shoulder on the susceptibility plot suggests a small amount of paramagnetic impurity. The data were fitted to a simple isotropic exchange Hamiltonian for two spin-coupled $S = 5/2$ centres [Equation (1)], using MAGMUN4.1.^[5]

$$H_{ex} = -J1\{S_1 \cdot S_2\} \quad (1)$$

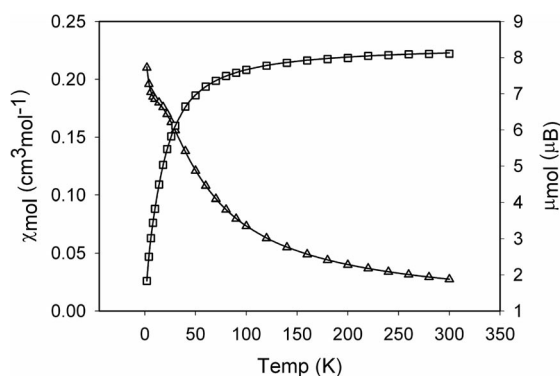


Figure 5. Variable-temperature magnetic data for **2**. See text for fitting parameters.

An excellent fit was obtained for $g = 2.00(1)$, $J = -3.9(1)$ cm^{-1} , $\text{TIP} = 0$ $\text{cm}^3 \text{mol}^{-1}$, $\rho = 0.031$ and $10^2 R = 0.33$ ($R = [\sum(\chi_{\text{obs}} - \chi_{\text{calc}})^2 / \sum \chi_{\text{obs}}^2]^{1/2}$). The J value is consistent with the structural arrangement of the two Mn^{II} centres connected by μ -O bridges with an Mn–O–Mn angle of 114.0°.^[6]

Variable-temperature magnetic data for **3** are shown in Figure 6 as plots of molar susceptibility and moment as a function of temperature. A characteristic maximum in χ_{mol} at 10 K signifies the presence of dominant intramolecular antiferromagnetic exchange.

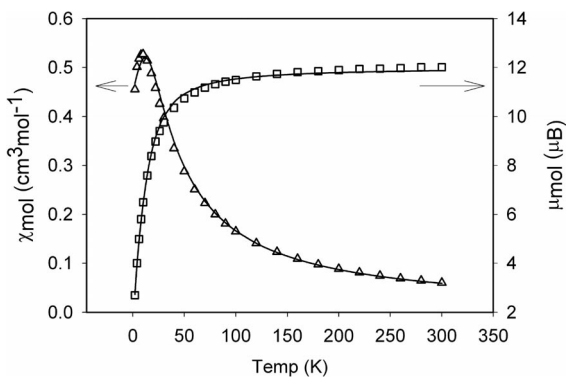


Figure 6. Variable-temperature magnetic data for **3**. See text for fitting parameters.

On examining the structure of **3** and the bridging connections within the dinuclear Mn^{II}₂ subunits, there is an obvious difference between the central and outer subunits based on the Mn–O–Mn bridging angles. All Mn–O–Mn angles in the central subunit are $< 90^\circ$, whereas the angles in the outer subunits are 103.6° and 115.6°. The classical exchange paradigm for O-bridged dinuclear species is associated with the magnitude of the M–O–M angle, particularly in the case of copper,^[7,8] and on the basis of overlap arguments involving metal ion orbitals and the oxygen p-orbitals, angles of around 90° represent a changeover region from ferromagnetic ($< 90^\circ$) to antiferromagnetic ($> 90^\circ$) behaviour. On this basis the magnetic behaviour of **3** was fitted to Equation (2), which assumes a positive J value for the central subunit ($J2$) and negative J values ($J1$) for the outer subunits. A good fit was obtained with the software package MAGMUN4.1,^[5] to give $g = 2.03(1)$, $J1 = -2.9(1)$ cm^{-1} , $J2 = 2.5(1)$ cm^{-1} and $\text{TIP} = 0$, $\theta = 0.4$ K ($10^2 R = 3.1$), and the solid line in Figure 6 was calculated with these parameters. The presence of both ferromagnetic and antiferromagnetic exchange in **3** is unusual but in agreement with orbital arguments based on M–O–M bridge angles. Examples of μ -O-bridged Mn^{II} dinuclear complexes exhibiting ferromagnetic exchange are rare. However, one example with two μ -O_{carboxylate} bridges and Mn–O–Mn bridge angles of 101.8° exhibits ferromagnetic exchange ($J = 0.462$ cm^{-1}), supported by theoretical calculations.^[9] The much smaller Mn–O–Mn angles in **3**, would be expected to lead to enhanced ferromagnetic exchange, as is observed.

$$H_{ex} = -J1\{S_1 \cdot S_2 + S_3 \cdot S_4\} - J2\{S_2 \cdot S_3\} \quad (2)$$

Variable-temperature magnetic data for **4** are shown in Figure 7 as plots of molar susceptibility and moment as a function of temperature. A characteristic maximum in χ_{mol} at 12 K signifies the presence of intramolecular antiferromagnetic exchange between the two Co^{II} centres. The moment drops steadily from 6.7 μ_B at 300 K to 1.05 μ_B at 2 K, which suggests a ground-state singlet. The orbital contributions to the magnetic properties of high-spin Co^{II} species ($S = 3/2$) are associated with the ⁴T_{1g} ground state and should be taken into account, unless their effect is effective.

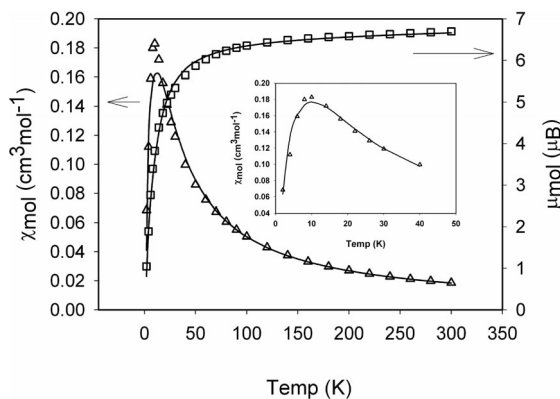


Figure 7. Variable-temperature magnetic data for **4**. See text for fitting parameters by using isotropic spin-only models (inset: fitting from 2 to 40 K).

tively quenched due to large distortions from octahedral symmetry.^[10,11] Complex **4** is quite distorted, and so an attempt was made to fit the data to a simple isotropic dinuclear exchange expression [Equation (1), $S = 3/2$], which assumes orbital-moment quenching. Surprisingly, a reasonably good fit was obtained over the full temperature range with MAGMUN4.1,^[5] to give $g = 2.43(8)$, $J = -5.3(1) \text{ cm}^{-1}$ and $\theta = -0.2 \text{ K}$ ($10^2R = 2.4$). The solid line in Figure 7 was plotted with these parameters.

The single-ion excited states for octahedral high-spin Co^{II} are well separated from the ground state, and the Kramer's doublet component of the $^4\text{T}_{1g}$ ground state, which arises from spin-orbit coupling, is the only one significantly populated at low temperatures ($< 30\text{--}40 \text{ K}$). Consequently, an isotropic fitting of the magnetic data to Equation (1) ($S = 3/2$) is perhaps considered more valid in this temperature range and should yield a more reasonable estimate of J . The magnetic data from $2\text{--}40 \text{ K}$ were therefore fitted to the isotropic exchange expression [Equation (1), $S = 3/2$] to give $g = 2.28(2)$, $J = -4.0(1) \text{ cm}^{-1}$, $\text{TIP} = 150 \times 10^{-6} \text{ cm}^3 \text{ mol}^{-1}$ and $\theta = -1 \text{ K}$ ($10^2R = 2.07$). The fit is shown in the inset of Figure 7. The reduced value of $-J$ using this treatment is reasonable, based on an expected overestimation of J when orbital contributions are ignored at higher temperatures.^[10,11] In an attempt to evaluate the single-ion Co^{II} contributions more thoroughly, Sakiyama's approach was adopted by using the software package MagSaki.^[12–14] Although an exactly comparable geometric model for the distortion in **4** was not available, an axial, anisotropic dinuclear Co^{II} model was used. A good fit was obtained for $J = -3.9 \text{ cm}^{-1}$, $g_z = 2.20$, $g_x = 4.95$, $\lambda = -158 \text{ cm}^{-1}$, $\kappa = 0.93$ and $\Delta = 793 \text{ cm}^{-1}$ ($10^2R = 2.3$) ($\lambda =$ spin-orbit coupling constant, $\kappa =$ orbital reduction factor, $\Delta =$ axial splitting parameter), and the result is shown in Figure 8. This model cannot be considered rigorous, but the parameters evaluated are reasonable compared with related dinuclear Co^{II} systems,^[10–14] and in particular the J value is entirely consistent with simpler models based on isotropic exchange (vide supra). It is clear from all fitting attempts that the antiferromagnetic exchange is based on the dinuclear structure and is propagated through the almost planar arrangement of the two N_2 triazole bridges, as expected.

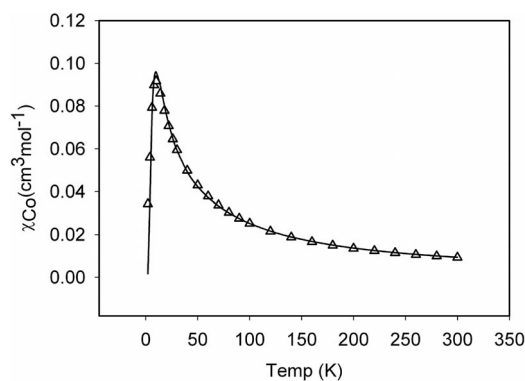


Figure 8. Variable-temperature magnetic data for **4**. See text for fitting parameters by using anisotropic model with orbital contributions.

Conclusions

The incorporation of multiple sites in a polyfunctional ligand creates donor complexity, and it is difficult to predict a priori which particular group will dominate on coordination. The hydrazone group has been shown to produce $\mu\text{-O}_{\text{hydrazone}}$ -bridged complexes in simple polytopic ligands with one type of substituent other than the hydrazone (e.g. poap, 2poap and related ligands Scheme 1) with grid systems prevailing.^[1] The introduction of carboxylate groups creates opportunities for new coordination motifs and the possibility of forming charge-neutral complexes. Ligands $\text{H}_2\text{L5}$ and $\text{H}_2\text{L6}$ also include heterocyclic components, which can bridge in their own right. With Mn^{II} and Co^{II} , three structural types were observed: 1D chain, dinuclear and tetranuclear, with short-range bridging through $\mu_2\text{-O}_{\text{hydrazone}}$, $\mu_2\text{-O}_{\text{carboxylate}}$ and $\mu_2\text{-triazole}$ -based groups. Spin-spin interactions through these bridges resulted in antiferromagnetic exchange in most cases, except for the central dimanganese portion of the Mn_4 chain cluster, where rare ferromagnetic coupling was observed as a result of the acute average Mn–O–Mn angles ($< 90^\circ$).

Experimental Section

Experimental Methods: Commercially available solvents and chemicals were used without further purification. Infrared (IR) spectra were obtained as Nujol mulls between KBr discs with a Mattson Polaris FT-IR instrument. Mass spectra were recorded with an Agilent 1100 Series LC/MSD in atmospheric-pressure chemical-ionization positive (APCI+) mode with methanol/acetonitrile mixtures as solvents. Variable-temperature magnetic data were collected with a Quantum Design MPMS55 Squid Magnetometer by using field strengths of $0.1\text{--}5 \text{ T}$ and in the temperature range of $2\text{--}300 \text{ K}$. Background corrections for the sample holder assembly and diamagnetic components of the complexes were applied.

Synthesis of Ligands

$\text{H}_2\text{L5}$: SOCl_2 (5 drops) was added to 2-pyrazinecarboxylic acid (Aldrich) (10.00 g, 0.0800 mol), dissolved in methanol (80 mL), and the mixture was heated to reflux for 3 d to give a clear brown solution. The solution was concentrated under reduced pressure to yield the corresponding methyl ester as a pink solid in quantitative yield. MS: $m/z = 139.0, 107.0$. IR: $\tilde{\nu} = 1720$ [$\nu(\text{CO})$ ester], 954 [$\nu(\text{pyrazine})$] cm^{-1} . The crude product was dissolved in methanol (200 mL), hydrazine monohydrate (4.97 g, 0.0993 mol) in methanol (10 mL) was added, and the mixture was heated to reflux for 24 h. 2-Pyrazinoic acid hydrazide was obtained as an off-white precipitate (yield 8.97 g, 81.2%), which was collected by filtration and washed with methanol ($2 \times 10 \text{ mL}$). MS: $m/z = 139.0, 121.0, 193.0$. IR: $\tilde{\nu} = 3305$ [$\nu(\text{NH})$], 3226 [$\nu(\text{NH})$], 1647 [$\nu(\text{CO})$ amide], 961 [$\nu(\text{pyrazine})$] cm^{-1} . 2-Pyrazinoic acid hydrazide (1.98 g, 0.0143 mol) was dissolved in methanol (100 mL) in a round-bottomed flask. Phenylglyoxylic acid (1.91 g, 0.0174 mol) was added with methanol (40 mL) to produce a clear light yellow solution. The solution was heated to reflux for approximately 24 h to yield $\text{H}_2\text{L5}$ as a white precipitate, which was collected by suction filtration and washed with methanol (yield 2.32 g, 60% based on 2-pyrazinoic acid hydrazide). MS: $m/z = 271.1$ [$\text{M} + \text{H}$] $^+$, 227.1, 225.1, 228.1. M.p. $220\text{--}225 \text{ }^\circ\text{C}$. IR: $\tilde{\nu} = 3214$ [$\nu(\text{NH})$], 1707 [$\nu(\text{CO})$], 1643, 1510 [$\nu(\text{CO})$, $\nu(\text{CN})$], 933 [$\nu(\text{pyrazine})$] cm^{-1} . $\text{C}_{13}\text{H}_{10}\text{N}_4\text{O}_3$ (270.25): calcd. C 57.80, H 3.70, N 20.74; found C 58.36, H 3.61, N 20.93.

HL6Na: Methyl-1*H*-1,2,4-triazole-3-carboxylate (Aldrich) (2.03 g, 0.0160 mol) was added to methanol (80 mL) in a round-bottomed flask to give a colourless solution. A solution of hydrazine hydrate (0.98 g, 0.020 mol) in methanol was added to the flask. The mixture was heated to reflux for 24 h to yield a white precipitate. The solid was isolated by suction filtration and washed with methanol to yield 1*H*-1,2,4-triazole-3-carbohydrazide (yield 1.86 g, 91% based on triazole carboxylate). MS: $m/z = 128.1$ [M + H]⁺, 73.1, 110.1, 70.1, 96.0. IR: $\tilde{\nu} = 3299$ [v(NH)], 3220 [v(NH)], 1671 [v(CO amide)] cm⁻¹. 1*H*-1,2,4-Triazole-3-carbohydrazide (1.86 g, 0.0146 mol) was dissolved in methanol (100 mL) in a round-bottomed flask to give a colourless solution. Sodium pyruvate (1.93 g, 0.0175 mol) and methanol (30 mL) were added, and the mixture was heated to reflux for 24 h to give a white precipitate. The white fluffy solid (HL6Na) was collected by suction filtration and washed with methanol (yield 3.12 g, 98% based on triazole hydrazide). M.p. >260 °C. IR: $\tilde{\nu} = 3351$, 3116 [v(NH)], 1691 [v(CO)], 1531 [v(CN)] cm⁻¹. C₆H₆N₅NaO₃ (219.13): calcd. C 32.73, H 3.18, N 31.82; found C 32.90, H 2.72, N 31.87.

Synthesis of Complexes

[C₂₈H₃₀MnN₈O₁₀]_n (1) and (C₁₃H₈N₄O₃)₂Mn₂(CH₃OH)(H₂O)₃ (2): Mn(CH₃COO)₂·4H₂O (0.10 g, 0.41 mmol) was dissolved in methanol (10 mL) in a round-bottomed flask. H₂L5 (0.10 g, 0.34 mmol) was added to methanol (10 mL), and the solution was warmed. The two mixtures were combined to give a cloudy orange solution. H₂O was added dropwise, but the precipitate still did not dissolve. The reaction mixture was then stirred and heated gently for 24 h. A cloudy orange solution resulted, which was gravity-filtered to give a clear light yellow filtrate, and an orange precipitate. Attempts to redissolve the precipitate were unsuccessful. The yellow filtrate was left to slowly concentrate at room temperature. Colourless crystals of **1** suitable for X-ray diffraction formed after 2 weeks (yield 45 mg, 16% based on metal salt). IR: $\tilde{\nu} = 3214$ [v(NH)], 1686 [v(CO amide)], 937 [v(pyrazine)] cm⁻¹. C₂₈H₃₀MnN₈O₆ (629.53): calcd. C 48.48, H 4.32, N 16.16; found C 47.83, H 4.08, N 16.42. On further standing, a small quantity of orange crystals (ca. 15 mg) of **2** was obtained from the mother liquor, which were also suitable for X-ray diffraction. C₂₇H₂₆Mn₂N₈O₁₀ (732.43): calcd. C 43.94, H 3.03, N 15.74; found C 44.25, H 3.57, N 15.30. The elemental

analysis indicates some water of solvation of the sample in comparison with the crystal chosen for X-ray analysis.

[(C₁₃H₉N₄O₃)₄(C₁₃H₈N₄O₃)₂Mn₄(H₂O)₅](H₂O)₂(CH₃OH)₂ (3): MnCl₂·4H₂O (0.090 g, 0.46 mmol) was dissolved in methanol (10 mL) in a round-bottomed flask. H₂L5 (0.10 g, 0.34 mmol) was added to the flask with a methanol/water (5:1) mixture (12 mL). The ligand did not dissolve initially, so triethylamine (4 drops) was added, which produced a dark yellow solution. The solution was gravity-filtered to give a dark yellow clear filtrate. The filtrate was left to slowly concentrate at room temperature. Orange, rod-shaped crystals suitable for X-ray diffraction formed after 1 week (yield 24.1 mg, 10.5% based on metal salt). IR: $\tilde{\nu} = 3219$ [v(NH)], 1691 [v(CO)], 1673, 1521 [v(CO, v(CN))], 933 [v(pyrazine)] cm⁻¹. (C₁₃H₉N₄O₃)₄(C₁₃H₈N₄O₃)₂Mn₄(H₂O)₅(H₂O)₃(CH₃OH)₂ (2040.28): calcd. C 47.05, H 3.72, N 16.47; found C 46.80, H 3.34, N 16.51.

[(C₆H₅N₅O₃)Co(H₂O)₂](H₂O)₄ (4): Co(NO₃)₂·4H₂O (0.16 g, 0.55 mmol) was dissolved in H₂O (5 mL) in a round-bottomed flask. H₂L6 (0.10 g, 0.46 mmol) was dissolved in H₂O (5 mL). The two solutions were combined and stirred at room temperature for 20 min to give a cloudy light pink solution. The solution was gravity-filtered to give a pink precipitate and a light pink, clear filtrate. The filtrate was left to slowly concentrate at room temperature. Red crystals suitable for X-ray diffraction formed after 2 weeks (yield 15.5 mg, 10.5% based on metal salt). IR: $\tilde{\nu} = 3415$, 3351, 3116 [v(NH), v(OH)], 1676 [v(CO)] cm⁻¹. (C₆H₅N₅O₃)₂Co(H₂O)₂·(H₂O)₄ (652.03): calcd. C 22.09, H 3.98, N 21.47; found C 22.19, H 3.68, N 21.75.

X-ray Crystallography: Crystals of **1–4** were mounted on low-temperature diffraction loops and measured with a Rigaku Saturn 70 CCD area detector with graphite-monochromated Mo-*K*_α radiation (Table 5). The structures were solved by direct methods^[15] and expanded by using Fourier techniques.^[16] Neutral atom scattering factors were taken from Cromer and Waber.^[17] Anomalous dispersion effects were included in $F_{\text{calcd.}}$ ^[18] and the values for $\Delta f'$ and $\Delta f''$ were those of Creagh and McAuley.^[19] The values for the mass attenuation coefficients are those of Creagh and Hubbell.^[20] All calculations were performed by using the CrystalStructure^[21,22] crystallographic software package except for refinement, which was performed by using SHELXL-97.^[15] All non-hydrogen atoms were

Table 5. Crystallographic details for **1–4**.

	1	2	3	4
Empirical formula	C ₂₈ H ₃₀ MnN ₈ O ₁₀	C ₃₀ H _{34.14} Mn ₂ N ₈ O _{11.07}	C ₈₀ H ₇₄ Mn ₄ N ₂₄ O ₂₇	C ₁₂ H ₂₆ Co ₂ N ₁₀ O ₁₄
<i>M</i>	693.53	793.78	2023.36	652.26
<i>T</i> [K]	153(2)	153(2)	153(2)	153(2)
Crystal system	monoclinic	triclinic	monoclinic	triclinic
Space group	<i>P</i> 2 ₁ / <i>c</i> (#14)	<i>P</i> 1̄ (#2)	<i>C</i> 2/ <i>c</i> (#15)	<i>P</i> 1̄ (#2)
<i>a</i> [Å]	9.357(8)	7.390(4)	28.616(9)	8.730(5)
<i>b</i> [Å]	16.212(14)	10.504(6)	18.375(5)	11.850(7)
<i>c</i> [Å]	12.732(11)	12.691(7)	21.610(7)	12.771(8)
<i>α</i> [°]	90	110.803(7)	90	114.910(6)
<i>β</i> [°]	127.562(14)	91.396(2)	125.292(3)	100.277(5)
<i>γ</i> [°]	90	108.263(7)	90	90.136(7)
<i>V</i> [Å ³]	1531(2)	864.2(8)	9275(5)	1174.6(12)
<i>Z</i>	2	1	4	2
<i>D</i> _{calcd.} [g/cm ³]	1.504	1.525	1.449	1.844
<i>μ</i> (Mo- <i>K</i> _α) [cm ⁻¹]	5.02	8.01	6.21	15.03
Reflections total	11994	8014	58060	9527
Reflections unique [<i>I</i> > 2.00σ(<i>I</i>)]	2733	3802	9131	4602
<i>R</i> _{int}	0.0650	0.0248	0.0956	0.0223
<i>R</i> ₁ [<i>I</i> > 2.00σ(<i>I</i>)]	0.0846	0.0317	0.0679	0.0253
<i>wR</i> ₂ (all reflections)	0.2736	0.0930	0.2043	0.0757

refined anisotropically. All O–H and N–H hydrogen atoms were located in difference-map positions. They were refined positionally with distance restraints and with fixed displacement ellipsoids (1.2 U_{eq} for N–H, and 1.5 U_{eq} for O–H). All other hydrogen atoms were introduced in calculated positions and refined on a riding model. Solution and refinement proceeded normally for **1**, **3** and **4**. For **2**, a complicated solvent model was required, however; excellent data quality revealed all protons in difference-map positions, and therefore allowed the refinement of several partial occupancy molecules. Of particular interest is the identity of O5, which was a member of two SHELXL parts; the first, at 0.464(4) occupancy, revealed that Mn1 was coordinated to a methanol molecule consisting of C15, H15(a,b,c), O5 and H5, with no uncoordinated lattice methanol present; the second, at 0.536(4) occupancy, revealed that Mn1 was coordinated to a water molecule consisting of O5, H5 and H5a. An additional lattice solvent methanol molecule was present, consisting of C16, H16(a,b,c), O6 and H6. CCDC-835343 (for **1**), -835344 (for **2**), -835345 (for **3**) and -835346 (for **4**) contain the supplementary crystallographic data for this paper. These data can be obtained free of charge from the Cambridge Crystallographic Data Centre via www.ccdc.cam.ac.uk/data_request/cif.

Acknowledgments

We thank the Natural Sciences and Engineering Research Council of Canada (NSERC) for financial support for this study.

- [1] L. N. Dawe, K. V. Shuvaev, L. K. Thompson, *Chem. Soc. Rev.* **2009**, 38, 2334 and references cited therein
- [2] a) Y.-B. Jiang, H.-Z. Kou, R.-J. Wang, J. Ribas, *Inorg. Chem.* **2005**, 44, 709; b) D. Maity, P. Mukherjee, A. Ghosh, M. G. B. Drew, C. Diaz, G. Mukhopadhyay, *Eur. J. Inorg. Chem.* **2010**, 807; c) S. Karmakar, O. Das, S. Ghosh, E. Zangrando, M. Johann, E. Rentschler, T. Weyhermüller, S. Khanra, T. K. Paine, *Dalton Trans.* **2010**, 39, 10920.
- [3] M. U. Anwar, L. K. Thompson, L. N. Dawe, *Dalton Trans.* **2011**, 40, 1437.
- [4] T. S. M. Abedin, L. K. Thompson, D. O. Miller, E. Krupicka, *Chem. Commun.* **2003**, 708.
- [5] MAGMUN4.1/OW01.exe is available as a combined package free of charge from the authors (<http://www.ucs.mun.ca/~lthomp/magmun>). MAGMUN has been developed by Dr. Zhiqiang Xu (Memorial University) and OW01.exe by Dr. O. Waldmann. We do not distribute the source codes.
- [6] H. Sakiyama, A. Sugawara, M. Sakamoto, K. Unoura, K. Inoue, M. Yamasaki, *Inorg. Chim. Acta* **2000**, 310, 163.
- [7] P. J. Hay, R. H. Thibeault, R. H. Hoffmann, *J. Am. Chem. Soc.* **1975**, 97, 4884.
- [8] W. H. Crawford, H. W. Richardson, J. R. Wasson, D. J. Hodgson, W. E. Hatfield, *Inorg. Chem.* **1976**, 15, 2107.
- [9] M. Wang, B. Wang, Z. Chen, *THEOCHEM* **2007**, 816, 103 and references cited therein.
- [10] G. deMunno, M. Julve, F. Lloret, J. Faus, A. Caneschi, *J. Chem. Soc., Dalton Trans.* **1994**, 1175.
- [11] S.-Y. Lin, G.-F. Xu, L. Zhao, J. Tang, G.-X. Liu, *Z. Anorg. Allg. Chem.* **2011**, 637, 720.
- [12] H. Sakiyama, *J. Comput. Chem. Jpn.* **2007**, 6, 123.
- [13] H. Sakiyama, *Inorg. Chim. Acta* **2006**, 359, 2097.
- [14] H. Sakiyama, *Inorg. Chim. Acta* **2007**, 360, 715.
- [15] SHELX97: G. M. Sheldrick, *Acta Crystallogr., Sect. A* **2008**, 64, 112–122.
- [16] DIRDIF99: P. T. Beurskens, G. Admiraal, G. Beurskens, W. P. Bosman, R. de Gelder, R. Israel, J. M. M. Smits, *The DIRDIF-99 program system*, Technical Report of the Crystallography Laboratory, University of Nijmegen, The Netherlands, **1999**.
- [17] D. T. Cromer, J. T. Waber, *International Tables for X-ray Crystallography*, The Kynoch Press, Birmingham, England, **1974**, vol. IV, Table 2.2 A.
- [18] J. A. Ibers, W. C. Hamilton, *Acta Crystallogr.* **1964**, 17, 781.
- [19] D. C. Creagh, W. J. McAuley, *International Tables for Crystallography*, vol. C, (Ed.: A. J. C. Wilson), Kluwer Academic Publishers, Boston, **1992**, p. 219–222, Table 4.2.6.8.
- [20] D. C. Creagh, J. H. Hubbell, *International Tables for Crystallography*, vol. C, (Ed.: A. J. C. Wilson), Kluwer Academic Publishers, Boston, **1992**, 200–206, Table 4.2.4.3.
- [21] *CrystalStructure 3.7.0: Crystal Structure Analysis Package*, Rigaku and Rigaku/MS, 9009 New Trails Dr., The Woodlands, TX 77381, USA, **2000–2005**.
- [22] *CRYSTALS Issue 10*: D. J. Watkin, C. K. Prout, J. R. Carruthers, P. W. Betteridge, Chemical Crystallography Laboratory, Oxford, UK, **1996**.

Received: July 18, 2011
Published Online: October 7, 2011